Monatsh Chem (2012) 143:1369–1378
DOI 10.1007/s00706-012-0805-6

ORIGINAL PAPER

A joint application of vibrational spectroscopic and quantum mechanical methods in quantitative analysis of baicalein structure

Tanja P. Brdarić · Zoran S. Marković · Dejan Milenković · Jasmina M. Dimitrić Marković

Received: 28 December 2011 / Accepted: 4 June 2012 / Published online: 6 July 2012

Abstract Theoretically predicted vibrational wavenumbers of baicalein were compared with available infrared (IR) and Raman experimental data. Assignments of the experimentally obtained normal vibrational modes were done using density functional theory calculations with M05-2X functional and the 6-311+G(2df,p) basis set implemented in the Gaussian 09 package. According to the results, the 1,700 to 1,400 cm^{-1} Raman and IR regions are associated with the double-bond character of the carbonyl group, aromatic in-plane skeletal vibrations, and aromatic character of the pyrone ring. In particular, the bands in the 1,650 to 1,550 cm^{-1} region represent the C=O and C2=C3 characteristic stretching modes. Most of the bands in the 1,500 to 650 cm^{-1} range involve C–C stretch, O–C stretch, and in-plane C–C–H, C–O–H, C–C–O, C–O–C, and C–C–C bending vibrations of the rings. Bands below 650 cm^{-1} are mostly assigned to different torsional modes of the rings. The applied method reproduced the experimental results with a high degree of accuracy.

Z. S. Marković
Department of Biochemical and Medical Sciences, State University of Novi Pazar, Vuka Karadžića bb, 36300 Novi Pazar, Republic of Serbia

T. P. Brdarić
Kirilo Savić Institute, Vojvode Stepe 51, 11000 Belgrade, Republic of Serbia

D. Milenković
Bioengineering Research and Development Center, 34000 Kragujevac, Republic of Serbia

J. M. Dimitrić Marković (✉)
Faculty of Physical Chemistry University of Belgrade, Studentski trg 12-16, 11000 Belgrade, Republic of Serbia
e-mail: markovich@ffh.bg.ac.rs

Keywords Baicalein · IR spectra · Raman spectra · M05-2X/6-311+G(2df,p) level of theory

Introduction

Besides the variety of internally developed defense mechanisms against reactive oxygen species, organisms rely also on some external factors including dietary substances, such as flavonoids, vitamins C and E, hydroquinones, and various sulfhydryl compounds. The flavonoid family is a vast and very important group of low-molecular-weight plant phenolics. Circumstantial evidence, provided by numerous investigations, points to their essential role in plant physiology, as they are involved in the light phase of photosynthesis, pigmentation, growth and reproduction, nitrogen fixation, regulation of iron channels associated with phosphorylation, resistance to pathogens and predators, ultraviolet (UV) protection of plants, and chemical defense [1–7].

By virtue of their unique electron-rich and highly conjugated chemical structure, flavonoids generally act as very good hydrogen and electron donors, which are very important determinants in antioxidant activity. Moreover, their radical intermediates are relatively stable due to delocalization effect and the lack of suitable sites for attack by molecular oxygen. Their pronounced antioxidant activity, closely related to a variety of their beneficial actions in vivo and in vitro, operates at different levels in the oxidative process, including scavenging lipid peroxyl radicals, chelation of metal ions able to promote radical formation through Fenton reactions, scavenging free radicals, removing oxidatively changed and damaged biomolecules, or regeneration of membrane-bounded antioxidants such as vitamin E [8–18].

In recent years, the chemical behavior of flavonoids as antioxidants has become the subject of very intense experimental and theoretical research, since the structure–properties relation has not yet been settled. In combination with experimental measurements, the various tools of computational chemistry have provided ways to disclose the relationship between the structure, properties, and performance of these very important molecules. This paper, as part of our ongoing investigations of flavonoid molecular structures [19–22], reports experimental and theoretical research into the baicalein (5,6,7-trihydroxy-2-phenyl-4*H*-chromen-4-one) structure by means of experimental IR and Raman spectroscopies and mechanistic calculations. In this way, by detailed vibrational band assignments, it is possible to provide good insight into the structural changes which appear upon all relevant flavonoid interactions. Found in the traditional Chinese medicinal herb Baikal skullcap (*Scutellaria baicalensis* Georgi), baicalein and its glycosidized form baicalin are two of its major bioactive flavone compounds. They are widely used in treatment of widespread and disease-related symptoms such as insomnia, fever, and perspiration. Baicalein has also been the subject of numerous studies which have given promising results in different areas, such as inhibition of iron-induced lipid peroxidation and anticancer, anti-inflammatory, and antioxidant activities [23–26].

Results and discussion

Geometry of baicalein

Different conformations of baicalein (Fig. 1) are implied by the possibility of rotation around the C2–C1′ single bond connecting the B and C rings and by the disposition that each –OH group can undergo in the molecule. Optimization at the M05-2X level of theory with the 6-311+G(2df,p) basis set yields as preferred structure a nonplanar conformation ($\tau = 23.4°$) in which the hydroxyl groups are oriented in such a way as to form the maximum number (three) of hydrogen bonds. This value for τ indicates that baicalein cannot use its full delocalization potential and is less active as scavenger. Nonplanarity can also be caused by the lack of 3-OH group, which causes a slight twist of the ring [27]. The energetic value for the rotation barrier around the torsional angle τ (16.2 kJ/mol), which leads to the B ring being perpendicular to the plane of the A and C rings, is much lower in comparison with the values of 24.7 kJ/mol for quercetin [21] and 23.0 kJ/mol for fisetin [20]. Obviously, the rotation around τ angle proceeds easily, and there is a very small energy gap between the two most stable conformations. This result suggests their probable coexistence.

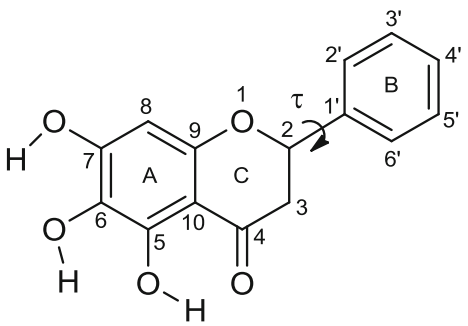

Fig. 1 Structural formula of baicalein

Equilibrium geometrical parameters of the absolute minimum are reported in Table 1, together with bond order values and data coming from crystallographic measurements [28]. If the known differences between the vacuum and condensed-phase environments are taken into account, the geometry appears to be quite well reproduced, and the small discrepancies are easily ascribable to the packing in the crystal. Significant geometrical differences were found only in the case of three hydrogen bonds. The O5–H5–O4 (1.689 Å), O6–H6–O5 (2.240 Å), and O7–H7–O6 (2.154 Å) hydrogen bonds present in the gas-phase minimum are significantly different from experimental values. The first one is shorter by 0.051 Å, and the other two are longer by 0.530 and 0.204 Å, respectively, in comparison with the experimental values. Also, it should be emphasized that this density functional theory (DFT) method overestimates the value of the dihedral angle between rings B and C by about 15°.

The Wiberg bond order analysis (Table 1), as well as small nonplanarity of the molecule, preclude a possible extended delocalization with a consequent good stabilization of the radical species, eventually originating from the hydrogen abstraction from the –OH groups of all the rings. As indicated by Rice-Evans et al. [29] and by van Acker et al. [18], the antioxidant properties of flavonoids can be derived just from their good delocalization possibilities.

IR and Raman spectra analysis

The vibrational spectra of polyhydroxylated flavones are generally very complex with the plurality of spectral bands mostly assigned to different modes of O–H vibrations, due to the fact that these molecules usually have several hydroxyl groups which are expected to have significant impact on the spectra appearance.

The experimentally obtained, theoretically calculated, and scaled band positions, wavenumbers, along with the corresponding assignments for the first 69 vibrational modes (of total 84) appearing in the 4,000 to 400 cm^{-1} region are listed in Table 2. Vibrational normal mode

Table 1 M05-2X/6-311+G(2df,p) geometrical parameters of the absolute minimum of baicalein in the gas phase

Bond lengths	Exp.	Gas phase	Wiberg bond order	Angles	Exp.	Gas phase
D(O1–C2)	1.353	1.347	1.011	A(C9–01–C2)	119.88	120.39
D(C2–C3)	1.360	1.348	1.631	A(O1–C2–C1′)	112.73	112.37
D(C3–C4)	1.432	1.440	1.122	A(O1–C9–C10)	121.17	120.38
D(C4–C10)	1.439	1.446	1.093	A(O1–C2–C3)	122.19	122.61
D(C5–C10)	1.414	1.403	1.246	A(C2–C3–C4)	121.05	121.06
D(C5–C6)	1.384	1.376	1.365	A(C3–C2–C1′)	125.07	125.02
D(C6–C7)	1.404	1.393	1.293	A(C3–C4–C10)	116.07	114.93
D(C7–C8)	1.392	1.385	1.364	A(C4–C10–C5)	121.79	120.81
D(C8–C9)	1.387	1.380	1.386	A(C4–C10–C9)	119.61	120.61
D(C9–O1)	1.369	1.364	0.964	A(C9–C10–C5)	118.58	118.58
D(C9–C10)	1.400	1.392	1.301	A(C10–C5–C6)	119.92	119.81
D(C2–C1′)	1.469	1.470	1.048	A(C5–C6–C7)	119.67	120.14
D(C1′–C2′)	1.399	1.392	1.371	A(C6–C7–C8)	121.55	121.21
D(C2′–C3′)	1.392	1.384	1.441	A(C7–C8–C9)	117.84	117.92
D(C3′–C4′)	1.393	1.386	1.430	A(C8–C9–C10)	122.26	122.34
D(C4′–C5′)	1.393	1.387	1.423	A(C8–C9–O1)	116.56	117.28
D(C5′–C6′)	1.386	1.383	1.449	A(C1′–C2′–C3′)	120.08	120.15
D(C6′–C1′)	1.402	1.392	1.367	A(C2′–C3′–C4′)	120.47	120.20
D(O4–C4)	1.260	1.238	1.541	A(C3′–C4′–C5′)	119.53	119.85
D(O5–C5)	1.348	1.341	1.064	A(C4′–C5′–C6′)	120.36	120.15
D(O6–C6)	1.362	1.364	0.993	A(C5′–C6′–C1′)	120.39	120.23
D(O7–C7)	1.350	1.347	1.045	A(C6′–C1′–C2′)	119.14	119.41
D(H5–O5)	0.970	0.993	0.623	A(C6′–C1′–C2)	120.27	120.52
D(H6–O6)	0.970	0.964	0.720	A(C2–C1′–C2′)	120.58	120.07
D(H7–O7)	0.970	0.965	0.728	A(C3–C4–O4)	122.76	123.18
DH(H5–O4)	1.740	1.689		A(C10–C4–O4)	121.17	121.88
DH(H6–O5)	1.710	2.240		A(C10–C5–O5)	122.13	122.00
DH(H7–O6)	1.950	2.154		A(C6–C5–O5)	117.93	118.18
				A(C5–C6–O6)	122.56	122.11
				A(C7–C6–O6)	117.76	117.75
				A(C6–C7–O7)	120.07	119.28
				A(C8–C7–O7)	118.39	119.51
				τ(O1–C2–C1′–C2′)	9.000	23.463

Distances in Å and valence angles in degrees. Experimental data are crystallographic measurements [40]

assignments were done on the basis of a best-fit comparison between the experimentally obtained and theoretically calculated spectra (Figs. 2, 3). Table 2 also lists relative descriptions of IR and Raman intensities, potential energy distribution (PED) values [30], and the description of the largest vibrational contributions to the normal modes. It can be seen that the calculated band positions provide a very good fit to the observed results, indicating correct mode assignments.

As baicalein possesses very low symmetry, belonging to the C1 symmetry group, its Fourier-transform (FT)-IR and Raman spectra are quite similar in appearance with slightly more bands present in the IR spectrum and some differences in relative intensities. The difference in number and intensity of the bands is the consequence of the Raman scattering effect itself. As implied by the low symmetry, the Raman and IR active vibrational modes also have rather similar assignments.

The most distinct and easily recognizable broad bands in IR and normal Raman (NR) spectra of phenols and polyphenols (also alcohols) are the bands assigned to different modes of O–H vibrations (Table 2). Although being predicted by DFT as three sufficiently intense (especially DFT-calculated IR intensities) bands (modes 84–82, Table 2), only two intense IR bands at 3,410 and 3,065 cm^{-1} are present. The first band, characteristic of weak hydrogen-bonding interaction, is assigned to mode 83 belonging to O–H stretching vibration of ring A (C7–OH). The second one is assigned to mode 82 (C5–OH), which is characteristic of OH groups involved in

Table 2 Experimental and calculated positions of the bands in the IR and Raman spectra of baicalein, assignments and intensities of the normal modes

Mode	Assignment	Exp. values		M05-2X/6-311+g(2df,p)			
		$\bar{\nu}_{IR}/cm^{-1}$	$\bar{\nu}_{R}/cm^{-1}$	$\bar{\nu}_{scaled}/cm^{-1}$	IR/Raman intensity	Raman activity	PED (%)
84	OH stretching (A) (C6–OH)			3,629.7	w/vw	66.2	ν_{OH} (99)
83	OH stretching (A) (C7–OH)	3,410		3,616.5	m/vw	114.6	ν_{OH} (99)
82	OH stretching (A) (C5–OH)	3,065		3,091.4	vw/vw	76.4	ν_{OH} (97)
81	CH stretching (A)			3,079.4	vw/v	68.3	ν_{CH} (99)
80	CH stretching (B)			3,064.6	vw/vw	247.3	ν_{CH} (98)
79	CH stretching (B)			3,060.1	vw/vw	22.1	ν_{CH} (95)
78	CH stretching (B)			3,053.5	vw/vw	76.2	ν_{CH} (83)
77	CH stretching (B)			3,046.3	vw/vw	114.4	ν_{CH} (95)
76	CH stretching (B)			3,036.3	vw/vw	40.8	ν_{CH} (95)
75	OH stretching (A)			3,017.7	vs/vw	133.1	ν_{CH} (86)
74	C=O stretching (C) CC stretching (A–C)	1,656	1,654	1,654.0	vs/m	206.5	$\nu_{C=O}$ (47) + δ_{COH} (10)
73	CC stretching (A, C) C=O stretching (C)	1,615	1,612	1,619.6	s/m	345.1	ν_{CC} (64)
72	CC stretching (B)			1,604.3	vw/vs	531.2	ν_{CC} (57) + δ_{CCH} (14)
71	CC stretching (A–B–C) OC stretching (A)	1,587	1,589	1,593.3	vw/w	150.1	ν_{CC} (44)
70	CC stretching (C) (C2=C3)	1,560	1,566	1,566.6	vw/s	318.0	ν_{CC} (44) + δ_{CCH} (11)
69	CC stretching (A, C) OC stretching (A)	1,504	1,507	1,495.1	w/w	144.5	ν_{CC} (18) + δ_{CCH} (34)
68	CC stretching (B)	1,471	1,466	1,474.8	vw/vw	9.2	ν_{CC} (13) + δ_{CCH} (59)
67	CC stretching (A, C) CCC bending (A, B) COH bending (A–C)	1,448	1,450	1,463.8	vs/vw	11.9	ν_{CC} (56)
66	CC stretching (B) CCH bending (B)	1,414	1,406	1,427.5	vw/vw	25.2	ν_{CC} (29)
65	OC stretching (A) CC stretching (B) COH bending (A)	1,388	1,381	1,388.3	w/vw	13.6	ν_{CC} (17) + δ_{CCH}(30)
64	CC stretching (A, C) COH bending (A)			1,365.9	vw/vw	67.0	ν_{CC} (67) + δ_{CCH} (12)
63	OC stretching (C) CC stretching (A) COH bending (A)	1,340		1,363.1	s/vw	73.4	ν_{CO} (12) + δ_{COH} (20)
62	OC stretching (C) COH bending (A)			1,304.0	s/vw	56.0	ν_{CO} (12) + δ_{COH} (20)
61	CC stretching (B) CCH bending (B)	1,296	1,280	1,298.8	vw/vw	0.9	ν_{CC} (10) + δ_{CCH} (65)
60	CC stretching (A) COH bending (A)			1,293.3	vw/vw	9.2	δ_{COH} (23)
59	CC stretching (B) CCH bending (B)			1,272.4	vw/vw	23.1	ν_{CC} (35) + δ_{CCH} (13)
58	COH bending (A) CCH bending (C)	1,242	1,248	1,245.2	w/vw	38.9	ν_{CO} (24) + δ_{COH} (21)

Table 2 continued

Mode	Assignment	Exp. values		M05-2X/6-311+g(2df,p)			
		$\bar{\nu}_{IR}/cm^{-1}$	$\bar{\nu}_{R}/cm^{-1}$	$\bar{\nu}_{scaled}/cm^{-1}$	IR/Raman intensity	Raman activity	PED (%)
57	CC stretching (C–B)	1,210	1,203	1,216.1	vw/s	241.9	ν_{CC} (34) + δ_{CCH} (33)
	CCH bending (C)						
	CCH bending (B)						
56	COH bending (A)			1,178.5	vw/vw	3.7	ν_{CC} (14) + δ_{COH} (45)
	CCH bending (A)						
55	COH bending (A)	1,181		1,170.3	vw/vw	64.0	ν_{CO} (26) + δ_{COH} (10) + δ_{CCH} (20)
	CCH bending (C)						
54	CCH bending (B)	1,161	1,160	1,155.0	vw/vw	7.9	ν_{CC} (11) + δ_{CCH} (72)
	CCH bending (A)						
53	CCH bending (A, B)			1,126.6	w/vw	2.9	δ_{CCH} (49)
	COH bending (A)						
52	CCH bending (B)	1,103	1,110	1,125.1	vw/vw	6.3	δ_{CCH} (72)
51	CCH bending (A)	1,084		1,078.3	vw/vw	10.9	ν_{OC} (58)
	CCC bending (A, C)						
	CCO bending (A, C)						
50	CCH bending (B)			1,067.0	vw/vw	0.1	ν_{CC} (17) + δ_{CCH} (43)
49	CCH bending (A, C)	1,031	1,032	1,054.1	m/vw	1.5	ν_{CC} (23) + δ_{CCO} (20) + δ_{CCH} (13)
	COH bending (A)						
48	CCH bending (B)	1,019		1,019.7	vw/vw	32.6	ν_{CC} (30) + δ_{CCH} (25) + δ_{CCC} (15)
47	CCH bending (A, B, C)			1,003.0	vw/vw	8.1	ν_{CC} (15) + δ_{CCH} (13)
46	CCH bending (B)	995	999	984.1	vw/vw	0.3	δ_{COH} (49)
45	CCH bending (B)	963		973.9	vw/vw	50.8	ν_{CC} (14) + δ_{CCC} (59)
44	CCH bending (B)			964.6	vw/vw	1.4	ν_{OC} (65) + δ_{CCH} (13)
43	CCH bending (B)	915		918.2	vw/vw	0.1	δ_{CCH} (39)
	CCC bending (A–C)						
	CCO bending (C–B)						
42	COC bending (C)	897		892.2	vw/vw	3.0	ν_{CC} (13) + δ_{CCC} (11) + δ_{COC} (13)
	CCH bending (C)						
	COH bending (A)						
41	CCH bending (A)			874.5	vw/vw	5.3	ν_{CC} (35) + δ_{CCH} (15)
	COH bending (A)						
	CCC bending (A)						
40	CCO bending (A–C)	852		848.7	vw/vw	0.9	δ_{CCC} (18) + δ_{CCO} (23)
	CCH bending (C)						
39	CCH bending (B)			832.4	vw/vw	3.0	δ_{HCC} (54)
	CCC bending (A)						
	CCO bending (C)						
38	CCH bending (A)	824		820.8	vw/vw	1.7	δ_{HCC} (74)
	CCC bending (B)						
37	CCO bending (A, C)			818.2	vw/vw	0.1	δ_{CCO} (35)
	CCC bending (B)						
36	CCC bending (A)	778		772.5	vw/vw	0.7	ν_{CC} (11) + δ_{CCC} (14)
	CCO bending (A–C)						
35	CCC bending (B)	748		760.8	vw/vw	2.4	ν_{CC} (15) + δ_{CCC} (11)
	CCH bending (B)						

Table 2 continued

Mode	Assignment	Exp. values		M05-2X/6-311+g(2df,p)			
		$\bar{\nu}_{IR}/cm^{-1}$	$\bar{\nu}_{R}/cm^{-1}$	$\bar{\nu}_{scaled}/cm^{-1}$	IR/Raman intensity	Raman activity	PED (%)
34	CCO bending (A, C)	734	729	707.9	vw/vw	0.2	δ_{CCH} (45)
	CCH bending (C)						
33	CCC bending (A, C)	706	712	693.9	vw/vw	3.9	ν_{OC} (13) + δ_{CCO} (12) + δ_{CCC} (13)
	CCO bending (A, C)						
	CCH bending (A, C)						
32	CCC bending (A, B)	682		687.4	vw/vw	4.8	δ_{CCO} (12) + δ_{CCC} (24)
	CCO bending (A, C)						
	CCH bending (B)						
31	CCC bending (B)	668		679.1	vw/vw	0.5	δ_{CCH} (22) + δ_{CCC} (28)
	CCH bending (B)						
30	CCH bending (B)	638	645	655.6	vw/vw	2.51	δ_{COC} (12) + δ_{CCH} (26)
	COC bending (A–C)						
29	CCC bending (A, B)			627.6	vw/vw	0.6	δ_{CCO} (15) + δ_{CCC} (32)
	CCO bending (B)						
28	CCOH torsion (A)	616	621	618.7	vw/vw	7.1	δ_{CCO} (30)
	CCCC torsion (A, C)						
27	CCCC torsion (A, B, C)			602.0	vw/vw	23.8	ν_{CC} (28) + δ_{CCC} (24)
	CCOH torsion (A)						
26	CCCH torsion (B)			596.9	vw/vw	9.2	δ_{CCC} (73)
	CCOH torsion (A)						
25	CCCH torsion (A–C)	595		590.2	vw/vw	0.5	τ_{HCCC} (21) + $\tau_{o.p.\ OCCC}$ (60)
24	CCCH torsion (A)	572	576	557.6	vw/vw	6.2	δ_{CCO} (55)
	CCCO torsion (A, C)						
23	CCCH torsion (A)	519	521	499.5	vw/vw	3.3	ν_{OC} (10) + δ_{CCC} (45)
	CCCO torsion (A, C)						
22	CCCH torsion (A, B, C)	487	481	472.7	vw/vw	1.0	δ_{CCC} (13) + τ_{CCCC} (14)
	CCCO torsion (A, C)						
21	CCCC torsion (A, B)	459		446.1	vw/vw	1.4	δ_{CCC} (14) + τ_{CCCC} (19)
	CCCO torsion (A, C)						
	CCCH torsion (A, B, C)						
20	HCCC torsion (A)	421	426	431.3	vw/vw	0.6	τ_{HOCC} (96)
19	CCOH torsion (A)			402.1	vw/vw	5.6	δ_{CCC} (19)
	CCCH torsion (A, B)						
	CCCO torsion (A, C)						
	CCCC torsion (A, B)						
18	CCCC torsion (B)			392.6	vw/vw	1.7	τ_{HCCC} (16) + τ_{CCCC} (19)
	CCCH torsion (B)						
17	CCCC o.p. torsion (B)			380.6	vw/vw	2.1	τ_{HOCC} (10) + $\tau_{o.p.\ CCCO}$ (48)
	CCCO o.p. torsion (B)						
	CCCC torsion (A, B)						
	CCCOC torsion (A–C)						

IR intensities are normalized with highest peak equal to 100. Raman intensities are calculated using the formulae for Raman intensity and then normalized to 100. Raman activity = Si of the normal mode

o.p. out-of-plane mode, *vw* very weak, *w* weak, *m* medium, *s* strong, *vs* very strong

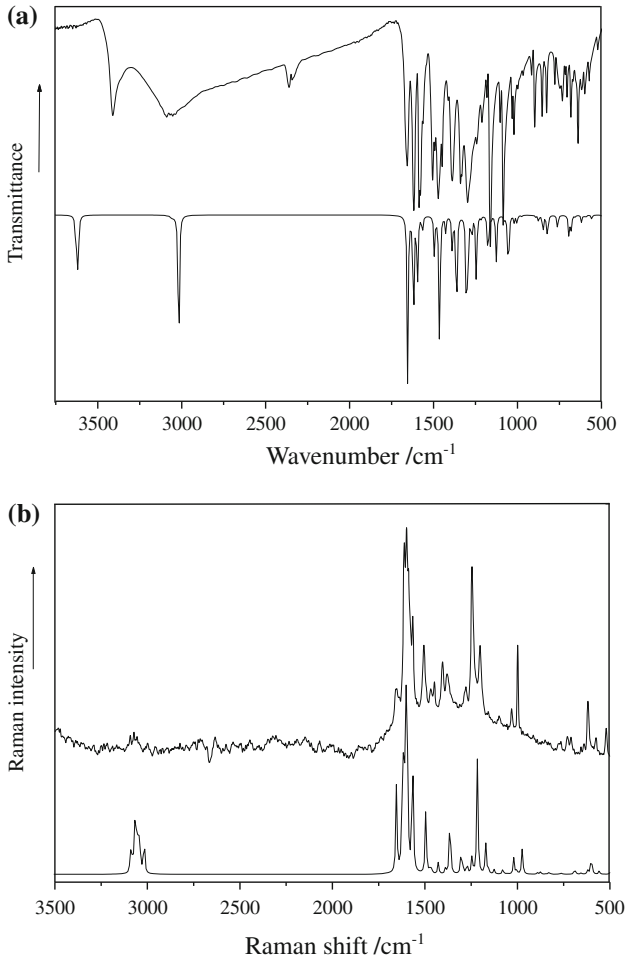

Fig. 2 Experimentally obtained (*top*) and theoretically calculated (*bottom*) IR (**a**) and Raman (**b**) spectra of baicalein

strong hydrogen bonding. These results are also confirmed by theoretical calculations (Table 1). The 3,850 to 3,200 cm^{-1} region is also very characteristic of various C–H stretching modes, but in the experimentally obtained IR and Raman spectra no bands are observed (Fig. 2). The lack of bands readily assignable to the various C–H stretching modes could arise from the possible interactions of adjacent molecules in the crystal phase [31, 32]. As obvious from Table 2, the largest vibrational contributions to the normal stretching modes of rings A, B, and C in the 3,850 to 3,200 cm^{-1} region are assigned solely to the stretching modes themselves. The rest of the vibrational modes are presented as the sum of various contributions.

The 1,700 to 1,400 cm^{-1} IR and Raman regions (Fig. 3) are generally associated with the double-bond character of the carbonyl group, aromatic in-plane skeletal vibrations, and aromatic character of the pyrone ring [32–35]. In the IR spectrum of baicalein, the most intense bands appear in the 1,656 to 1,560 cm^{-1} region (1,654 to 1,567 cm^{-1} scaled DFT values), usually involving a combination of the C=O stretching (1,656 and 1,615 cm^{-1}), C2=C3 stretching (1,560 cm^{-1}), and C–C stretching (1,656, 1,615, 1,587, and 1,560 cm^{-1}) vibrations. In the Raman spectrum these bands appear in the 1,654–1,566 cm^{-1} region, almost at the same positions as corresponding bands in the IR spectrum (1,654 and 1,612 cm^{-1}; 1,566 cm^{-1}; 1,654, 1,612, 1,589, and 1,566 cm^{-1}). As baicalein lacks a hydroxyl group at the C3-position the frequencies of both the C=O and C2=C3 stretching modes are slightly increased and positioned at higher values compared with 3-OH substituted flavones such as quercetin and some other flavonols

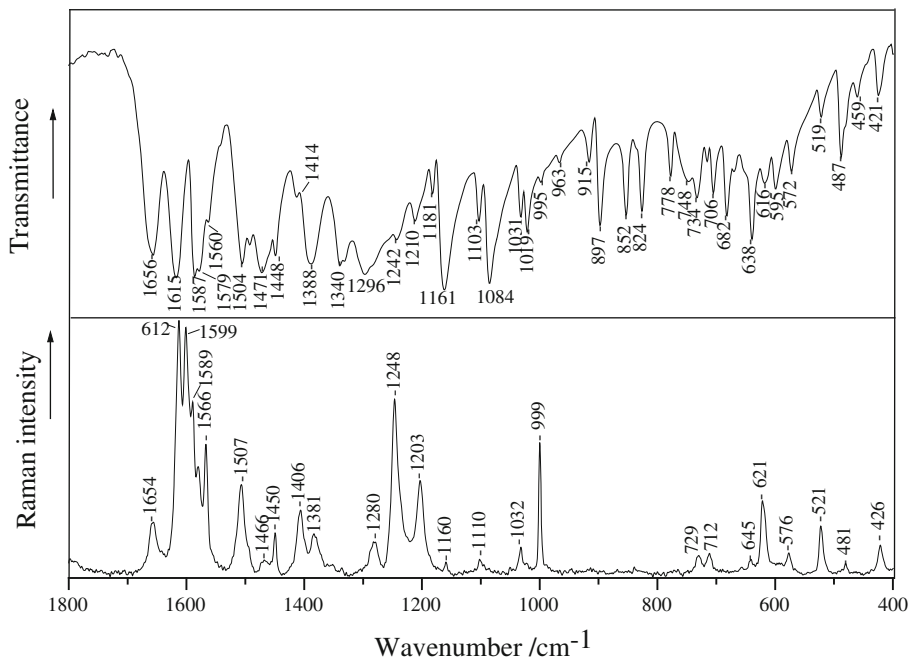

Fig. 3 Region from 1,800 to 400 cm^{-1} of the IR (*top*) and Raman (*bottom*) spectra of baicalein (potassium bromide matrix)

[35–37]. Most of the bands between 1,500 and 1,000 cm^{-1} involve C–C stretching, O–C stretching, and in-plane C–C–H, C–O–H, C–C–O, and C–C–C bending vibrations of the rings. The plurality of less intense bands which appear only in the IR spectrum below 1,000, 1,019 cm^{-1} (1,020 cm^{-1} by DFT), 995 (984 cm^{-1} by DFT), 963 cm^{-1} (974 cm^{-1} by DFT), 915 cm^{-1} (918 cm^{-1} by DFT), 897 cm^{-1} (892 cm^{-1} by DFT), 852 cm^{-1} (849 cm^{-1} by DFT), 824 cm^{-1} (821 cm^{-1} by DFT), 778 cm^{-1} (772 cm^{-1} by DFT), 748 cm^{-1} (761 cm^{-1} by DFT), 734 cm^{-1} (708 cm^{-1} by DFT), 716 cm^{-1} (694 cm^{-1} by DFT), 682 cm^{-1} (687 cm^{-1} by DFT), 668 cm^{-1} (679 cm^{-1} by DFT), and 638 cm^{-1} (679 cm^{-1} by DFT), is predominantly assigned to the C–C–C, C–C–H, C–C–O, C–O–C, and C–O–H deformation modes of all three rings. Bands that appear below 650 cm^{-1} in both IR (616, 572, 519, 487, 459, and 421 cm^{-1}) and Raman spectra (621, 576, 521, 481, –, and 426 cm^{-1}) are assigned to in-plane C–C–C–C, C–C–O–H, C–C–C–H, and C–C–C–O torsional modes of the rings. DFT-predicted wavenumber values for the various torsional modes are, as all the rest of calculated modes, in very good agreement with experimentally measured values (618, 558, 499, 472, 446, and 431 cm^{-1}). Band around 400 cm^{-1}, predicted only by DFT calculations, is assigned to out-of-plane C–C–C–C and C–C–C–O torsional modes of the B ring.

Conclusions

The results of the applied M05-2X/6-311+G(2df,p) density functional method in determination of the spectroscopic and electronic features of baicalein point to a nonplanar molecule, characterized by an extended delocalization and conjugation of the *p* electrons, which exists in one stable form containing three hydrogen bonds. Spectral assignments, done on the basis of a best-fit comparison between the experimentally obtained and theoretically calculated IR and Raman spectra, match quite well, indicating DFT calculations as a very accurate source of normal mode assignments.

Experimental

Computational methods

The conformations of different baicalein forms were fully optimized with the new local density functional method (M05-2X), developed by the Truhlar group [38, 39], by using the 6-311+G(2df,p) basis set as implemented in the Gaussian 09 package [40]. This new hybrid meta exchange–correlation functional is parameterized for nonmetallic compounds, yielding satisfactory overall performance for main-group thermochemistry and thermochemical kinetics, as well as organic, biological, and noncovalent interactions [38, 41, 42]. Moreover, this functional has been proven to give much better correlation between experimental and calculated band wavenumbers compared with DFT/B3LYP functional with 6-31G(d,p) basis set.

The vibrational frequencies were obtained from diagonalization of the corresponding M05-2X Hessian matrices. The nature of the stationary points was determined by analyzing the number of imaginary frequencies: 0 for minimum and 1 for transition state. Relative energies were calculated at 298 K.

The vibrational modes were assigned on the basis of PED analysis [30] using VEDA 4 program with its visualization interface [43]. Normal coordinate analysis of baicalein was carried out to obtain a more complete description of the molecular motions involved in the fundamentals. The calculated vibrational wavenumbers were scaled with the uniform scaling factor of 0.9444 [44–46] to obtain better match between calculated and experimental wavenumber values.

Potential energy surfaces were obtained in relation to the torsion angle τ defined by the C3–C2–C1′–C2′ atoms (Fig. 1) between rings B and C. The torsion angle τ was scanned in steps of 10° without constraints on all other geometrical parameters. The effects of the following torsion angle rotations were also studied: C4–C5–OH, C5–C6–OH, and C6–C7–OH. Afterwards, the structures were further optimized without any constraint around each potential minimum. Particular attention was devoted to the DFT interpretation of the reactivity of OH groups in the parent molecule, and the radicals and cations formed after H-removal from the molecule.

Natural bond orbital (NBO) analysis [47–50] of baicalein was also performed. The Wiberg bond orders [51] were calculated using the GenNBO program. It should be noted that the Wiberg bond order (sometimes referred to as the Wiberg bond index) is equal to 1 and 2 for pure single and double bonds, respectively. In the case when a bond participates in some π-electron conjugation, its Wiberg bond order will assume a value between 1 and 2, with values closer to 2 indicating stronger double-bond character.

IR spectra

IR spectra were recorded on a Thermo Nicolet 6700 FT-IR spectrometer with attenuated total reflectance (ATR). The spectra were recorded in the middle IR region from 4,000 to 400 cm^{-1}, which is important for monitoring the structural changes of molecules. The spectral resolution was 2 cm^{-1}. Baicalein (Merck, USA) was studied in potassium bromide matrix with sample:KBr ratio of 1 mg:150 mg.

Raman spectra

Raman spectra were recorded on a Thermo Scientific Nicolet Almega XR Raman spectrometer. The spectra were obtained in the region from 3,500 to 500 cm^{-1} directly from the pure powder sample. A 532-nm laser was used for sample illumination, enabling spectral resolution of 2 cm^{-1}. The laser output was kept at 10 mW. Each spectrum was collected after 1 s of exposure. The number of exposures was ten. Fluorescence correction was applied.

The theoretical Raman intensities (I_i^R) were derived from the computed Raman scattering activities using the following equations [52]:

$$I_i^R = C(\upsilon_0 - \upsilon_i)^4 \upsilon_i^{-1} B_i^{-1} S_i, \quad (1)$$

where B_i is a temperature factor which accounts for the intensity contribution of excited vibrational states, and is represented by the Boltzmann distribution:

$$B_i = 1 - \exp\left(-\frac{h\upsilon_i c}{kT}\right). \quad (2)$$

In Eq. (1), υ_0 is the wavenumber of the laser excitation line ($\upsilon_0 = 18{,}797$ cm^{-1}, corresponding to wavelength of 532 nm), υ_i is the normal mode wavenumber (cm^{-1}), while S_i is the Raman scattering activity of normal mode Q_i. The theoretical Raman intensity, I_i^R, is given in arbitrary units (C is a constant equal to 10^{-12}). In Eq. (2) h, k, c, and T are the Planck and Boltzmann constants, speed of light, and temperature in Kelvin, respectively. The factor B_i was assumed to be 1; otherwise, the calculated Raman intensities for the bands below 300 cm^{-1} were extremely overestimated in comparison with experiment [53].

Acknowledgments The authors acknowledge financial support by the Ministry of Science of Republic of Serbia (grant no. 172015).

References

1. Harborne JB, Williams CA (2000) Phytochemistry 55:481
2. Cody V, Middleton E, Harborne JB (1986) Plant flavonoids in biology and medicine: biochemical, pharmacological, and structure-activity relationships. Alan R Liss, New York
3. Cody V, Middleton EJR, Harborne JB, Beretz A (1988) Plant flavonoids in biology and medicine II: biochemical, cellular, and medicinal properties. Alan R Liss, New York
4. Lambert JD, Sang SM, Yang CS (2007) Chem Res Toxicol 20:583
5. Rechner AR, Kuhnle G, Bremner P, Hubbard GP, Moore KP, Rice-Evans CA (2002) Free Radical Biol Med 33:220
6. Lee KW, Lee HJ (2006) BioFactors 26:105
7. Cook NC, Samman S (1996) Nutr Biochem 7:66
8. Rice-Evans C, Miller N (1996) Biochem Soc Trans 24:790
9. Pietta PG (2000) J Nat Prod 63:1035
10. Cao G, Sofic E, Prior R (1997) Free Radical Biol Med 22:749
11. Haslam E (1996) J Nat Prod 59:205
12. Larson RA (1997) Naturally occurring antioxidants. Lewis Publishers, CRC Press LLC, Boca Raton
13. Pietta PG (1997) In: Rice-Evans CA, Packer L, Dekker M (eds) Flavonoids in health and disease. Marcel Dekker, New York
14. Sies H (1986) Angew Chem Int Edit 25:1058
15. Diplock AT (1994) In: Rice-Evans CA, Burdon RH (eds) Free radical damage and its control. New comprehensive biochemistry, vol 28. Elsevier, Amsterdam
16. Husain SR, Cillard J, Cillard P (1987) Phytochemistry 26:2489
17. Rice-Evans C, Miller NJ, Bolwell PG, Bramley PM, Pridham JB (1995) Free Radic Res 22:375
18. van Acker SABE, van de Berg DJ, Tromp MNJL, Griffioen DH, van Bennekom WP, van der Vijgh WJF, Bast A (1996) Free Radical Biol Med 20:331
19. Marković ZS, Mentus SV, Dimitrić Marković JM (2009) J Phys Chem A 113:14170
20. Marković ZS, Dimitrić Marković JM, Milenković D, Filipović N (2011) J Mol Model 17:2575
21. Marković ZS, Dimitrić Marković JM, Doličanin ĆB (2010) Theor Chem Acc 127:69
22. Wolniak M, Oszmianski J, Wawer I (2008) Magn Reson Chem 46:215
23. Perez CA, Wei Y, Guo M (2009) J Inorg Biochem 103:326
24. Li BQ, Fu T, Dongyan Y, Mikovits JA, Ruscetti FW, Wang JM (2000) Biochem Biophys Res Commun 276:534
25. Duen-Suey C, Jie-Jen L, George H, Cheng-Ying H, Yan-Jyu T, Tzeng-Fu C, Joen-Rong SJ (2007) J Agric Food Chem 55:649
26. Kitamura K, Honda M, Yoshizaki H, Yamamoto S, Nakane H, Fukushima M, Ono K, Tokunaga T (1998) Antiviral Res 37:131
27. Rezabal E, Mercero JM, Lopez X, Ugalde JM (2007) J Inorg Biochem 101:1192
28. Hibbs DE, Overgaard C, Gatti T, Hambley W (2003) New J Chem 27:1392
29. Rice-Evans CA, Miller NJ, Paganga G (1996) Free Radical Biol Med 20:933
30. Munos RA, Panchenko YN, Koptev G, Stepanov NF (1970) J Appl Spectrosc 12:428
31. Jurasekova Z, Garcia-Ramos JV, Domingo C, Sanchez-Cortes S (2006) J Raman Spectrosc 37:1239
32. Teslova T, Corredor C, Livingstone R, Spataru T, Birke RL, Lombardi JR, Canamares MV, Leona M (2007) J Raman Spectrosc 38:802
33. Varsanayi G (1974) Assignments for vibrational spectra of 700 benzene derivates. Adam Hilger, London
34. Torreggiani A, Jurasekova Z, Sanchez-Cortes S, Tamba M (2008) J Raman Spectrosc 39:265
35. Jurasekova Z, Torreggiani A, Tamba M, Sanchez-Cortes S, Garcia-Ramos JV (2009) J Mol Struct 918:129
36. Torreggiani A, Trinchero A, Tamba M, Taddei P (2005) J Raman Spectrosc 36:380
37. Wang M, Teslova T, Xu F, Spataru T, Lombardi JR, Birke RL (2007) J Phys Chem C 111:3038
38. Zhao Y, Schultz NE, Truhlar DG (2008) Theor Chem Acc 120:215
39. North MA, Bhattacharyya S, Truhlar DG (2010) J Phys Chem B 114:14907
40. Frisch MJ, Trucks GW, Schlegel HB, Scuseria GE, Robb MA, Cheeseman JR, Zakrzewski VG, Montgomery Jr JA, Stratmann RE, Burant JC, Dapprich S, Millam JM, Daniels AD, Kudin KN, Strain MC, Farkas O, Tomasi J, Barone V, Cossi M, Cammi R, Mennucci B, Pomelli C, Adamo C, Clifford S, Ochterski J, Petersson GA, Ayala PY, Cui Q, Morokuma K, Malick AD, Rabuck KD, Raghavachari K, Foresman JB, Cioslowski J, Ortiz JV, Babou AG, Stefanov BB, Liu G, Liashenko A, Piskorz P, Komaromi I, Gomperts R, Martin RL, Fox DJ, Keith T, Al-Laham MA, Peng CY, Nanayakkara A, Challacombe M, Gill PMW,

Johnson B, Chen W, Wong MW, Andres JL, Gonzalez C, Head-Gordon M, Replogle ES, Pople JA (2009) Gaussian 09, Revision A.1-SMP, Gaussian Inc, Wallingford, CT
41. Zhao Y, Schultz NE, Truhlar DG (2005) J Chem Phys 123:161103
42. Zhao Y, Schultz NE, Truhlar DG (2006) J Chem Theory Comput 2:364
43. Jamróz MH (2004) Vibrational energy distribution analysis. VEDA 4, Warsaw
44. Wong MW (1996) Chem Phys Lett 256:391
45. Scott AP, Radom LJ (1996) J Phys Chem 100:16502
46. Jalkanen KJ, Stephens PJ (1991) J Phys Chem 95:5446
47. Reed AE, Weinstock RB, Weinhold F (1985) J Chem Phys 83:735
48. Glendening E, Reed AE, Carpenter JE, Weinhold F (2012) NBO Version 3.1
49. Reed AE, Curtiss LA, Weinhold F (1988) Chem Rev 88:899
50. Carpenter JE, Weinhold F (1988) J Mol Struct 169:41
51. Wiberg KB (1968) Tetrahedron 24:1083
52. Unsalan O, Erdogdub Y (2009) J Raman Spectrosc 40:562
53. Wysokinsk R, Hernik K, Szostak R, Michalska D (2007) Chem Phys 333:37